PHYSICAL REVIEW B VOLUME 48, NUMBER 17 1 NOVEMBER 1993-I

Neutron-diffraction studies of zinc-blende MnTe epitaxial films and MnTe/ZnTe superlattices: The effect of strain and dilution on a strongly frustrated fcc antiferromagnet

T. M. Giebultowicz
Physics Department, University of Notre Dame, Notre Dame, Indiana 46556
and National Institute of Standards and Technology, Gaithersburg, Maryland 20899

P. Kłosowski,* N. Samarth,† H. Luo, and J. K. Furdyna
Physics Department, University of Notre Dame, Notre Dame, Indiana 46556

J. J. Rhyne
Missouri University Research Reactor, Columbia, Missouri 65211

(Received 12 March 1993)

We report neutron-diffraction studies of antiferromagnetism in various forms of epitaxially grown zinc-blende (ZB) MnTe: in semibulk (~ 1 μm thick) single-crystal films of pure MnTe, in its magnetically diluted derivative $Zn_{1-x}Mn_xTe$ with $0.695 < x < 1$, and in strongly strained very thin (30–300 Å) single-crystal MnTe layers in MnTe/ZnTe superlattices. ZB Mn chalcogenides are unique examples of fcc Heisenberg antiferromagnets (AF) with dominant nearest-neighbor interactions. Such a lattice is one of the basic models of topologically frustrated spin systems. Only ZB MnS can be obtained through natural crystallization (and only in a fine powder form, which seriously limits the scope of possible studies on this system). The single-crystal forms of MnTe obtained using molecular-beam epitaxy have made it possible to study the influence of strain on a frustrated fcc antiferromagnet. We observe that such built-in strain strongly affects the domain structure as well as the phase-transition behavior. Furthermore, high-resolution x-ray diffraction reveals pronounced magnetostriction effects in the MnTe films. Both neutron as well as x-ray data indicate a rather unusual effect of a strong temperature shift in the relative populations of two inequivalent AF domain states, and a magnetosctriction mechanism underlying this phenomenon is proposed. Finally, the data obtained on $Zn_{1-x}Mn_xTe$ films complement the results of previous magnetic studies on bulk forms of this material with $x \leq 0.68$.

I. INTRODUCTION

Zinc-blende (ZB) Mn chalcogenides offer unique examples of Heisenberg fcc antiferromagnets with strongly dominant nearest-neighbor (NN) exchange interactions. The dominance of the NN exchange in these compounds results from the anion-cation configuration in the ZB structure. This arrangment consists of NN cation tetrahedra with an anion inside [Fig. 1(a)], which gives rise to a strong superexchange coupling between these cations.[1,2] Since the "superexchange paths" between the next-nearest neigbors (NNN) and more distant magnetic pairs always involve more than one anion,[3] the exchange coupling between such spins is decidely weaker than between the NN spins (the ratio of the NN and NNN exchange constants J_1/J_2 in these systems is usually estimated[4,2] to be between 5 and 10). This is in contrast with the situation in most other known fcc antiferromagnets, which are usually of the NaCl type.[5] In that case the anions are located between the NNN magnetic cations [Fig. 1(b)], thus giving rise to a dominating NNN superexchange. In fact, there are only a few other known examples of NN fcc antiferromagnets (AF), e.g., $KIrCl_6$, the pyrite-type MnS_2, $MnSe_2$, $MnTe_2$ family,[6–8] or Cu and Ag which show nuclear spin ordering at ultralow temperatures.[9] However, all those systems exhibit significant magnetic anisotropy or dipolar coupling, and hence cannot be regarded as pure Heisenberg antiferromagnets. In contrast, in ZB Mn chalcogenides there is essentially no crystal field anisotropy (Mn^{2+} is an *s*-state ion) and the dipolar components are negligibly small, so that these compounds are close realizations of the Heisenberg model.

The sole representative of the Mn chalcogenides family which crystallizes naturally in the ZB structure is

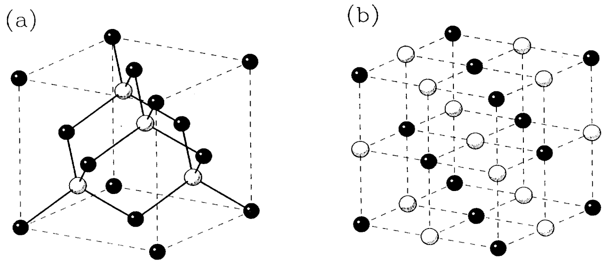

FIG. 1. Chemical unit cells in the zinc-blende (a) and the NaCl (b) structure.

0163-1829/93/48(17)/12817(17)/$06.00

β-MnS.[10,11] ZB phases of MnSe and MnTe have only recently been obtained[12,13] through the application of molecular-beam epitaxy (MBE). In this paper we report the results of magnetic neutron-diffraction studies of various epitaxial forms of ZB MnTe, such as strained-layer MnTe/ZnTe superlattices, "semibulk" MnTe single-crystal films, as well as films of a weakly magnetically diluted derivative of this system, $\mathrm{Zn}_{1-x}\mathrm{Mn}_x\mathrm{Te}$.

The organization of this paper is as follows. In Secs. I A–I C we review earlier magnetic studies of ZB Mn chalcogenides and their derivatives, the developments in MBE growth of such systems, and the application of neutron diffraction in studies of these epitaxial forms. In Sec. II we recapitulate the AF structures and phase-transition effects seen in ZB antiferromagnets. Sample preparation and experimental procedures are described in Sec. III. In Sec. IV we present the results of measurements and their interpretation for each of the specimen types investigated, and in Sec. V we discuss and summarize the results of the present study. Some details of neutron diffraction in AF structures of the type seen in Mn chalcogenides, and of nuclear diffraction in superlattices made up of ZB materials, are discussed in Appendices A and B.

A. ZB Mn chalcogenides and their derivatives

The AF fcc lattice with only NN interactions is an important theoretical model because of its inherent "frustration"—i.e., the inability to simultaneously satisfy all the AF bonds. Such a lattice has a strongly degenerate magnetic ground state, and most of its configurations are nonperiodic.[14] The degeneracy may be removed by additional symmetry-breaking perturbations, intrinsic or artificially induced—e.g., by weak Dzyaloshinskii-Moriya anisotropic coupling,[15] strain, or weak dilution by a nonmagnetic component.[16] Such circumstances can lead to a rich variety of collinear and noncollinear configurations,[15,16] and in the case of stronger dilution they may produce spin-glass-like states.[17,18]

Although the properties of frustrated fcc systems have been the subject of many theoretical studies, the limited availability of naturally existing prototypes resulted in relatively little experimental work in this field. The only naturally occurring ZB Mn chalcogenide, β-MnS, can be obtained only in powder form. Although neutron-diffraction experiments on β-MnS powders have provided crucial insights into the spin structure[10] and the nature of the AF phase transition[11] in this system, such specimens do not offer much opportunity of studying other intriguing properties of a frustrated fcc spin lattice—e.g., its behavior under the influence of anisotropic strain fields, or in the case of weak or strong magnetic dilution.

The two other representatives of the Mn-VI family, MnSe and MnTe, normally occur in different structures (NaCl and NiAs, respectively[5]), in which the magnetic sublattices are not frustrated. However, as has been discovered some time ago, one can obtain a number of new ternary ZB derivatives of these materials by alloying them with various II-VI ZB compounds (e.g., CdTe, ZnSe). Such alloys—e.g., $\mathrm{Zn}_{1-x}\mathrm{Mn}_x\mathrm{Se}$, $\mathrm{Hg}_{1-x}\mathrm{Mn}_x\mathrm{Te}$—can be regarded as *magnetically diluted* forms of the "hypothetical" ZB MnSe and MnTe, and some of them ($\mathrm{Zn}_{1-x}\mathrm{Mn}_x\mathrm{Te}$ and $\mathrm{Cd}_{1-x}\mathrm{Mn}_x\mathrm{Te}$) retain the ZB structure up to Mn concentration as high as $x \leq 0.70$. It should be noted that due to their many properties which are highly interesting from the viewpoint of semiconductor physics,[19–21] these materials are commonly referred to in the literature as diluted magnetic semiconductors, or semimagnetic semiconductors (DMS, SMSC). However, in the present paper we avoid that terminology and use instead the general chemical formula $A^{\mathrm{II}}_{1-x}\mathrm{Mn}_x B^{\mathrm{VI}}$, because our attention is focused on the *magnetic* properties of these systems (and the name "DMS" might misleadingly suggest that their magnetism is ruled by their semiconducting nature). In fact, as far as the basic interaction mechanisms between the magnetic spins are concerned, the $A^{\mathrm{II}}_{1-x}\mathrm{Mn}_x B^{\mathrm{VI}}$ alloys should be classified together with magnetic insulators, since in the case of these materials the overwhelming part of the Mn^{2+}-Mn^{2+} coupling arises from superexchange effects, whereas the mechanisms specific to semiconductors (e.g., the Bloembergen-Rowland exchange[22]) play only a marginal role.[1]

The emergence of the "DMS" systems has stimulated considerable interest in studies of diluted frustrated FCC lattices. As predicted by theoretical considerations,[23,24,17,14] a strong ground-state degeneracy combined with random dilution should lead to the formation of spin-glass states. The $A^{\mathrm{II}}_{1-x}\mathrm{Mn}_x B^{\mathrm{VI}}$ alloys indeed show many characteristic features of spin glasses, such as the absence of long-range spin order[25] (LRO), pronounced cusps in magnetic susceptibility vs T,[26,27] and a frequency dependence of the cusp temperature[28]—which is a particularly important signature of a spin-glass state. Such behavior is observed throughout a wide alloy compositon range, even for Mn concentrations as high as $x = 0.65$. On the other hand, neutron-scattering data from $A^{\mathrm{II}}_{1-x}\mathrm{Mn}_x B^{\mathrm{VI}}$ alloys with $x = 0.40 - 0.70$ indicate that these systems show much similarity to ordered antiferromagnets. For instance, although there is no *true* spin LRO, the short-range AF spin-spin correlations seen in these systems[29] reach as far as 30–70 Å, which is an unrealistically large correlation length for a true spin glass. Also, as seen by inelastic neutron-scattering measurements,[30] magnetic excitations in these systems show much more resemblance to dispersive magnons occurring in ordered spin systems than to diffusive and hydrodynamic modes characterizing disordered magnetism. Thus, as suggested by neutron data, $A^{\mathrm{II}}_{1-x}\mathrm{Mn}_x B^{\mathrm{VI}}$ alloys with high Mn concentrations should be rather classified as "cluster antiferromagnets."

A reasonable explanation of the conflicting data obtained by various experimental methods seems to be that the $A^{\mathrm{II}}_{1-x}\mathrm{Mn}_x B^{\mathrm{VI}}$ systems have an unusually broad crossover region between a true spin-glass state occuring below $x \approx 0.30$, and a true LRO AF phase expected to occur in the x region inaccessible by bulk growth. However, the *exact* nature of the magnetic phase in the crossover region still remains puzzling, as attempts of constructing a comprehensive model which would provide at least a semiquantitative consistent interpretation of all the experimental facts (such as, e.g., the "activated dynamics model" proposed in Ref. 28) have never brought about a fully satisfying result. A serious obstacle in such efforts has been the lack of data from the high-x region—in particular, of information about the location of the SRO-LRO boundary in the magnetic phase diagram, and about details of the SRO$\leftrightarrow$LRO transition process itself. Over the last years it has therefore become clear that further progress in understanding the magnetism of the $A^{\mathrm{II}}_{1-x}\mathrm{Mn}_xB^{\mathrm{VI}}$ systems hinges critically on access to the magnetic concentration region above the x=0.70 bulk growth limit.

B. MBE-grown Mn chalcogenides

The only way to accompish this goal is by exploiting the nonequilibrium low-temperature growth technique of molecular-beam epitaxy (MBE). As has been established some time ago, the ZB structure of the $A^{\mathrm{II}}_{1-x}\mathrm{Mn}_xB^{\mathrm{VI}}$ systems can be preserved up to much higher Mn concentrations than in the case of bulk growth if they are prepared in the form of thin films on ZB substrate materials (e.g., GaAs), or in the form of superlattices consisting of alternating $A^{\mathrm{II}}_{1-x}\mathrm{Mn}_xB^{\mathrm{VI}}$ layers and pure ZB compound layers (e.g., ZnSe, ZnTe). One of the first successes in this area was the growth of of $\mathrm{Zn}_{1-x}\mathrm{Mn}_x\mathrm{Se}$ epilayers and $\mathrm{Zn}_{1-x}\mathrm{Mn}_x\mathrm{Se}$/ZnSe superlattices on (001) GaAs substrates.[12] In the latter, the ZB structure of $\mathrm{Zn}_{1-x}\mathrm{Mn}_x\mathrm{Se}$ can be preserved even up to x=1. This initial accomplishment was soon followed by many other new developments in the growth of pure ZB MnSe and its derivatives—for instance, of ZB single crystal $\mathrm{Cd}_{1-x}\mathrm{Mn}_x\mathrm{Se}$ films[29] with $x\leq0.75$, and quite recently, of MnSe/ZnTe superlattices.[31,32] Another significant development in the MBE growth of $A^{\mathrm{II}}_{1-x}\mathrm{Mn}_xB^{\mathrm{VI}}$ materials has been the preparation of a variety of new systems containing ZB MnTe in pure and magnetically diluted forms. These include MnTe/ZnTe multilayers, single-crystal MnTe films with "semibulk" thicknesses (up to $\sim$1 μm or even more), as well as $\mathrm{Zn}_{1-x}\mathrm{Mn}_x\mathrm{Te}$ single-crystal films from the previously inaccessible Mn concentration region, $0.70\leq x\leq 1$.[13,33–37]

The MBE-grown $A^{\mathrm{II}}_{1-x}\mathrm{Mn}_xB^{\mathrm{VI}}$ and $\mathrm{Mn}B^{\mathrm{VI}}$ structures not only complement the spectrum of previously available diluted systems, but in addition such specimens open up many opportunities for entirely new experimental studies of frustrated fcc antiferromagnets. For instance, the systems prepared in multilayer form (e.g., MnSe/ZnSe, MnSe/ZnTe, and MnTe/ZnTe) provide excellent prototypes for investigating the behavior of such spin systems under the influence of strong anisotropic strain fields. Due to the relatively large lattice mismatch between the lattices of Mn-VI and II-VI compounds, the magnetic layers in these artificial structures exhibit tetragonal distortions from cubic symmetry (c/a=0.94–1.06) that would be impossible to obtain by externally applied stresses on bulk materials. Further, as interdiffusion effects in the Mn-VI/II-VI heterostructures appear to be relatively weak, one can produce good quality superlattices with the magnetic layer thicknesses even as small as 3–5 monolayers.[38] This offers the opportunity of investigating the so far unexplored crossover region between 3D (three-dimensional) and 2D antiferromangnetism in frustrated fcc lattices.

C. Neutron-diffraction studies of $\mathrm{Mn}B^{\mathrm{VI}}$ and $A^{\mathrm{II}}_{1-x}\mathrm{Mn}_xB^{\mathrm{VI}}$ epitaxial structures

Neutron diffraction is an extremely well-suited experimental tool for the study of magnetism in the new MBE-grown $A^{\mathrm{II}}_{1-x}\mathrm{Mn}_xB^{\mathrm{VI}}$ and $\mathrm{Mn}B^{\mathrm{VI}}$ structures. Because of the very small volume of the magnetic material, the use of many experimental techniques appropriate for studying bulk $A^{\mathrm{II}}_{1-x}\mathrm{Mn}_xB^{\mathrm{VI}}$ alloys is not straightforward. For instance, magnetization signals from these AF thin films and multilayers are so weak that they can be detected only by SQUID magnetometry.[39] The interpretation of such data also presents a problem because of the overwhelming diamagnetic contribution from the substrate. In contrast, the AF nature of the $A^{\mathrm{II}}_{1-x}\mathrm{Mn}_xB^{\mathrm{VI}}$ systems presents a considerable advantage from the point of view of neutron-diffraction studies, because in such a case the magnetic maxima occur at different Q-space points than the Bragg reflections produced by the substrate, and by the epitaxial structure itself. Another highly helpful circumstance is that most of the $A^{\mathrm{II}}_{1-x}\mathrm{Mn}_xB^{\mathrm{VI}}$ epitaxial forms appear to be of good crystalline quality. Hence, experiments on these systems can be done on conventional single-crystal diffractometers and do not require the application of special methods such as polarization analysis—which is sometimes necessary in the case of ferromagnetic thin-film and superlattice systems.

In a series of recent papers we have reported neutron-diffraction data from several MnSe-based epitaxial forms. Our experiments on ZB $\mathrm{Cd}_{1-x}\mathrm{Mn}_x\mathrm{Se}$ single-crystal films with x=0.70 and 0.75 have revealed the onset of a LRO AF phase which has never before been observed in any $A^{\mathrm{II}}_{1-x}\mathrm{Mn}_xB^{\mathrm{VI}}$ system.[29] Studies of MnSe/ZnTe superlattices have provided the first detailed picture of the AF structure which forms in the strained MnSe layers.[38] One interesting fact revealed by our experiments is that the AF phase transition in these layers is clearly of *second order*, whereas renormalization-group theoretical considerations predict[40,41] a *first-order* transition for this class of systems, and such behavior is indeed seen[11] in ZB β-MnS. The observed change of the transition order can be attributed to a strong deviation from the fcc symmetry in the MnSe layers ($c/a \approx 1.05$) resulting from the lattice mismatch stress. Another effect that can also be attributed to strain is the formation of only one specific AF domain structure in these layers.[38] The superlattice systems have also made possible systematic studies of antiferromagnetism in the MnSe layers as a function of their *thickness.* Here an important observation[38] was that the AF structure occurring in these layers does not change its character even at the thickness level of only three monolayers ($\sim$ 9 Å). The only effect which can be interpreted as signalizing the approch of the 2D limit is a marked decrease of the Néel temperature in the case of the thinnest layers.

In this paper we report the results of diffraction experiments on several epitaxial systems containing ZB MnTe. An important advantage of this material is that it can be obtained not only in a superlattice form, but also in the form of *single-crystal epilayers* with micron thicknesses. The crystalline quality of such films appears to be very good (in contrast to this, and for reasons which are not yet entirely clear, attempts of growing thick ZB MnSe specimens have never been successful—the crystalline quality of the epilayers usually deteriorates after the deposition of only ~100 Å of the material). Also, diffraction checks of these specimens do not show any significant differences between the MnTe lattice periodicity in the growth direction and in the film plane, indicating that the bulk of the material is essentially strain-free. On the other hand, in the case of MnTe/ZnTe superlattices the MnTe layers exhibit a very similar lattice distortion ($c/a \approx 1.05$) as the MnSe layers in the MnSe/ZnSe structures. As shown by our experiments, the MnTe/ZnTe multilayers also exhibit a second-order AF phase transition and the same preferred orientation of AF domains as previously observed[38] in the former systems, and now a comparison with the data obtained on the "thick" MnTe films provides a direct proof that this behavior is indeed caused by strain effects. In addition to that, high-resolution diffraction measurements on the MnTe films have made it possible to detect another interesting magnetoelastic phenomenon in this material—namely, a substantial magnetostriction that leads to a temperature shift in the populations of nonequivalent domain states in the low-T AF phase. Finally, diffraction experiments on several $\mathrm{Zn}_{1-x}\mathrm{Mn}_x\mathrm{Te}$ epitaxial layers with x=0.695–0.975 have provided information about the magnetic phase diagram of an $A^{\mathrm{II}}_{1-x}\mathrm{Mn}_x B^{\mathrm{VI}}$ system in the $0.70 < x < 1$ region.

II. THEORETICAL BACKGROUND

A. Spin ordering in frustrated fcc lattices

The fcc spin lattice with dominant NN AF interactions may exhibit two different types of order, depending on the sign of the weak NNN coupling. These two configurations, which are commonly referred to as type I (AFM-I) and type III (AFM-III) structures after the original paper on antiferromagnetism in fcc lattices by Anderson,[42,43] are displayed schematically in Figs. 2(a) and 2(b), respectively. As shown in the figures, both these arrangements consist of AF sheets of spins on (001)-type planes (represented in the plots by the shaded squares). Within the sheets all NN spins are antiferromagnetically coupled. It is important to notice, however, that in the case of such planar AF arrangement in the fcc lattice each spin has always an equal number of "frustrated" and "unfrustrated" NN's located in the adjacent sheets. This leads to zeroing of the effective coupling beetwen the "A" and "B" planes. Hence, the only interplanar coupling is that occurring between the *second-nearest* sheets (i.e., A-A, B-B coupling), maintained by the NNN interaction. Consequenly, this latter interaction determines the sheet stacking sequence: ferromagnetic NNN interaction leads to parallel orientation of spins in the A-A, B-B planes, which is the AFM-I structure [Fig. 2(a)]. AF NNN coupling, on the other hand, produces A-$\bar{A}$-A-..., B-$\bar{B}$-B-... stacking seqences (where the bar denotes spin reversal), and then the structure becomes AFM-III type [Fig. 2(b)].

The schemes in Figs. 2(a) and 2(b) depict the simplest collinear (or "Ising") AFM-I and AFM-III ground-state configurations. In the figure the spins point along one of the cubic axes, but in fact their orientation is not restricted to any particular direction. There are two distinct ground-state degeneracies in such structures: first, the AF sheets may form on (100), (010), or (001) planes, giving equivalent energy per spin. Second, in Heisenberg systems—where not only "up" and "down" spin states are allowed—spins may be rotated on every second sheet by an arbitrary but identical angle: since, as noted, all interactions between the "A" and "B" sheets sum up to zero, such an operation does not change the energy balance. The ground state is therefore continuously degenerate, and has an infinite number of noncollinear configurations. A "canted" AFM-III arrangement corre-

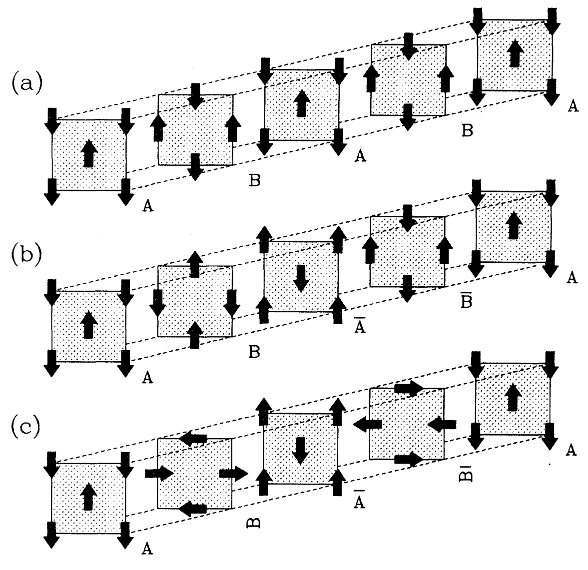

FIG. 2. Simple ground-state configurations in fcc spin lattices with dominant NN AF exchange interactions. The structures consist of sheets of antiferromagnetically coupled spins on (001)-type planes (symbolized by the shaded squares). For clarity, the sheets are shifted apart along the [001] direction. Ferromagnetic NNN interaction leads to parallel orientation of spins in the second-nearest sheets (a), which is commonly referred to as the type I (AFM-I) structure. AF NNN coupling leads to an antiparallel orientation (b), which is the type III (AFM-III) structure. Because the coupling energy between the spins in adjacent sheets sums to zero, a rotation of all the B sheets at the same angle with respect to the A sheets does not change the magnetic energy per spin. An example of a noncollinear AFM-III configuration corresponding to a 90° rotation of the B sheets (known as the Keffer structure) is displayed in plot (c).

sponding to a rotation of the B planes by 90°, often referred to as the "Keffer[15] ordering scheme," is displayed as an example in Fig. 2(c). In addition to that, such lattices have an infinite number of more complex multi-**k** noncollinear ground-state configurations which we will not discuss here (for details, see, e.g., Ref. 44). Because the exchange interactions in ZB Mn-VI compounds are all antiferromagnetic, these systems are supposed to exhibit AFM-III structure. This type of order has been indeed observed in β-MnS by Corliss and co-workers[10] in their well-known paper on antiferromagnetism in polymorphous forms of MnS, and AFM-III LRO or SRO has been found later in all ZB $A^{\mathrm{II}}_{1-x}\mathrm{Mn}_xB^{\mathrm{VI}}$ and $\mathrm{Mn}B^{\mathrm{VI}}$ bulk as well as epitaxial systems investigated by neutron diffraction. However, the problem of whether these systems are collinear or not still remains open. As has been determined by Corliss *et al.*, the spin directions β-MnS are confined to the planes of the AF sheets, but the in-plane spin orientation could not be established from their powder data. Shortly afterwards Keffer[15] has pointed out that in the absence of any significant magnetic anisotropy the spins should actually be perpendicular to the sheet planes because this orientation minimizes the energy of dipolar interactions. In-plane orientation, as argued, may indicate the presence of a Dzyaloshinskii-Moryia (DM) component ($\propto \mathbf{S}_i \times \mathbf{S}_j$) in the spin-spin exchange, because this interaction is allowed in β-MnS due to the lack of inversion symmetry in the ZB structure. In fact, the DM interaction favors perpendicular NN orientation, and thus it would stabilize the canted AFM-III structure shown in Fig. 2(c).

B. Critical behavior of AFM-III systems

The most widely used approach to phase-transition phenomema in magnetic crystals is the renormalization-group theoretical analysis of the critical region. This approach involves construction of a multidimensional order parameter and its associated Landau-Ginzburg-Wilson (LGW) Hamiltonian, and investigation of the system behavior under the renormalization-group transformation. Such analysis was applied to AF systems in the 1970s, most notably by Mukamel and collaborators.[40,41,45] For AFM-III systems with spins lying in the plane of the AF sheets Bak and Mukamel[40,45] derived a 12-dimensional order parameter, and consequently predicted a first-order magnetic phase transition, since the renormalization transformation does not have a stable fixed point. Such transition has been indeed observed in β-MnS.[11] However, it has been noted that under symmetry-breaking anisotropies the fixed point may become accessible and the second-order behavior may be restored.[46,47] The transition of that kind has been indeed observed[48] in MnO, a fcc antiferromagnet with AFM-II structure (a second kind of AF ordering, according to the Anderson's classification)—where the uniaxial stress causes a distortion and breaks the cubic symmetry, leading to second-order behavior. However, no such experiments have yet been reported for any AFM-III systems.

Bak and Mukamel's theory predicts that only an AFM-III system with spins perpendicular to the AF sheets may exhibit a second-order phase transition, but the first-order transition is expected to occur in the case of all "in-plane" arrangements, collinear as well as of the Keffer type. Hence, the observation of the first-order transition in β-MnS does not bring us any closer to answering to the question concerning the existence of DM interactions in this system.

III. SAMPLES AND INSTRUMENTS

A. Sample growth

The thin-film and epilayer samples investigated in the present study were fabricated at the University of Notre Dame using a Riber MBE apparatus equipped with effusion sources of Mn, Zn, and Te. All samples were grown on (001) GaAs substrates after the deposition of 2 μm ZnTe buffer layers in order to diminish the lattice-mismatch stresses (a_{GaAs}=5.65 Å, a_{ZnTe}=6.10 Å, and a_{MnTe}=6.34 Å). The MnTe and $\mathrm{Zn}_{1-x}\mathrm{Mn}_x\mathrm{Te}$ epilayers had a thickness of 1 μm. We have investigated two MnTe specimens and a nuber of $\mathrm{Zn}_{1-x}\mathrm{Mn}_x\mathrm{Te}$ samples with various Mn concentrations, listed in Table I.

The Mn concentration in the $\mathrm{Zn}_{1-x}\mathrm{Mn}_x\mathrm{Te}$ epilayers was determined by precise x-ray diffraction measurements of the lattice parameters. As has been found from lattice parameter studies in $A^{\mathrm{II}}_{1-x}\mathrm{Mn}_xB^{\mathrm{VI}}$ alloys, all these materials strictly obey the Vegard law within the Mn concentration ranges available by bulk growth. In particular, measurements on two MnTe derivatives, $\mathrm{Zn}_{1-x}\mathrm{Mn}_x\mathrm{Te}$ and $\mathrm{Cd}_{1-x}\mathrm{Mn}_x\mathrm{Te}$ with $x \leq 0.70$ have yielded the following $a(x)$ dependences:[49]

$$a_{\mathrm{Zn}_{1-x}\mathrm{Mn}_x\mathrm{Te}} = (6.102 + 0.238x)\ \text{Å} \tag{1}$$

and

$$a_{\mathrm{Cd}_{1-x}\mathrm{Mn}_x\mathrm{Te}} = (6.487 - 0.146x)\ \text{Å}. \tag{2}$$

The fact that both these empirical relations give almost identical values of the lattice parameter for pure MnTe

TABLE I. Summary of the MnTe and $\mathrm{Zn}_{1-x}\mathrm{Mn}_x\mathrm{Te}$ films investigated: the Mn concentrations, the Néel temperatures, and the order of the AF phase transition as suggested by the magnetic reflection intensity vs T.

Sample	x (%)	T_N (K)	Phase trans. order
MT-1	100	66.7 ± 0.3	1st
MT-2	100	66.7 ± 0.3	1st
ZMT-1	97.5 ± 0.5	63.8 ± 0.5	1st
ZMT-2	94.2 ± 0.5	62.0 ± 0.5	1st
ZMT-3	93.8 ± 0.5	61.7 ± 0.5	1st
ZMT-4	85.0 ± 0.5	56.4 ± 0.5	2nd
ZMT-5	81.5 ± 0.5	52.5 ± 0.5	2nd
ZMT-6	72.5 ± 0.5	46.5 ± 0.5	2nd[a]
ZMT-7	69.5 ± 0.5	45.0 ± 1.0	2nd[a]

[a] Transition to a SRO phase.

indicates that in the x region above x=0.70 there is also no deviation from linearity in $a(x)$. The values of x obtained from Eq. (1) for our specimens are listed in Table I. The MnTe/ZnTe superlattice samples were obtained by a controlled process, in which the quality of the epitaxial growth was monitored by observing the reflection high-energy electron diffraction (RHEED) patterns, and the number of MnTe and ZnTe monolayers deposited was determined from oscillations of the RHEED intensity. We have investigated two superlattice samples with relatively thin MnTe layers, and one specimen in which the MnTe layer thickness was made as large as possible, in order to achieve a "macroscopic" thickness. The number of bilayers and the MnTe and ZnTe layer thicknesses for each sample is given in Table II. The lattice parameter data for the strained MnTe layers are listed in Table III.

B. Neutron and x-ray diffraction instruments

The samples were investigated using conventional single-crystal neutron and x-ray techniques. Neutron studies were performed at the 20 MW research reactor at National Institute of Standards and Technology with a (002) pyrolitic graphite (PG) monochromator and analyzer fixed for elastic scattering, and a PG filter in the incident beam. An incident energy of 13.7 or 14.8 meV with 40 arc minute collimation throughout was used for most of the experiments. The samples were placed in a variable-temperature He cryostat, and were oriented with the (100) in-plane axis perpendicular to the scattering plane, which enabled the observation of $(0kl)$ reflections.

The x-ray diffraction measurements were done on a standard diffractometer equipped with crystal monochromator and analyzer using filtered $K\alpha$ Cu or Mo radiation. The lattice parameter data were obtained from measurements of the (004) reflections in symmetric reflection geometry at room temperature. Magnetostriction effects in MnTe films were investigated by observing higher-order $(00l)$ reflections at large 2θ angles. In such measurements the samples were mounted in a variable-temperature Displex refrigerator with a Be window.

IV. EXPERIMENTS AND DATA ANALYSIS

A. MnTe epilayers

The results of test x-ray measurements indicate a high crystalline quality of the epitaxial MnTe films. The width of the rocking curves show that the mosaic spread in these single-crystal films is of the order of 0.2°, which is a lower value than usually observed in bulk $A^{\rm II}_{1-x}{\rm Mn}_xB^{\rm VI}$ crystals. The MnTe lattice parameter inferred from $\theta - 2\theta$ scans was $a = 6.346 \pm 0.002$ Å, in close agrement with the value reported by Durbin *et al.*[13] The reflections observed in $\theta - 2\theta$ scans exhibited a slight broadening, corresponding to a $\Delta a \approx 0.008$ Å spread in the a value. Such a broadening may result from weak residual stresses caused by differences in thermal expansion coefficients of the substrate, the ZnTe buffer, and the epilayer material (it should be noted that the growth process takes place at $\sim 400\,^{\circ}$C). However, the small value of Δa indicates that strong stresses produced by a MnTe and ZnTe lattice mismatch are relieved within a relatively thin (several hundred Å) interface area. The strain-free nature of the films is also indicated by neutron-diffraction measurements of the lattice constants in the growth direction (c) and in the growth plane (a_{xy}) which do not show any difference beyond the standard error (because the GaAs substrate is almost transparent to neutrons, the determination of a_{xy} by this method is quite straigthforward, while it poses a problem in x-ray diffraction).

TABLE II. Summary of the MnTe/ZnTe superlattices investigated in this work.

Sample ID	ZnTe thickness (monolayers)	MnTe thickness (monolayers)	Number of repeats
SL-1	18	10	100
SL-2	18	20	100
SL-3	330	130	10

Low-T diffraction scans revealed two families of AFM-III reflections, $(0k\frac{n}{2})$, and $(0\frac{n}{2}l)$. The first of these correspond to AFM-III domains in which the AF sheets are *parallel* to the MnTe film plane, and the second to domains in which the sheets are *perpendicular* to the film plane and to the (100) scattering plane. This is shown schematically in Fig. 3, where these two domain configurations are denoted as "Z" and "Y" arrangements, respectively. There is also a third possible domain state denoted as "X" in the figure—namely, one with the AF sheets perpendicular to the film plane but *parallel* to the scattering plane. Such domains gives rise to a family of $(\frac{n}{2}kl)$ reflections which all lie beyond the (100) plane, so that they could not be seen in the experimental geometry used by us. However, because the "X" and "Y" domains are strictly equivalent from the point of view of the specimen symmetry, one can presume that the population of these two states is approximately equal. This has been confirmed experimentally by test measurements.

The magnetic reflections showed no detectable broadening beyond the instrumental linewidth in any direction, indicating that the AFM-III order seen in the films is of true long-range nature, and that the size of the domains is >1000 Å (i.e., the detectability level determined by the Q resolution in our measurements).

Although the occurrence of $(0k\frac{n}{2})$ as well as $(0\frac{n}{2}l)$ peaks in the diffraction patterns shows that all possible AFM-III domain types are present in the films, the intensity of these reflections indicates that there is considerable asymmetry in the population of these states. Namely, at the lowest T about 2/3 of the domains are of the "Z" type, and the remaining 1/3 are "X" and "Y" domains. Surprisingly, this asymmetry tends to increase when T is raised, and close to the phase-transition temperature the "Z" domains constitute an overwhelming majority. We will return to this effect when discussing magnetostriction data in Sec. IV B.

The integrated intensities of several $(0k\frac{n}{2})$ reflections observed in experiments on one of the investigated samples are listed in Table IV. These intensities are com-

TABLE III. Lattice parameter data for strained MnTe layers in the MnTe/ZnTe superlattices studied in this work, obtained from the analysis of nuclear and magnetic diffraction spectra.

Sample	MnTe lattice parameter[a] in Å From nuclear diffraction a_{xy}	 c	 From magnetic diffraction a_{xy}	 c
SL-1	6.137 ± 0.005	6.520 ± 0.020	6.130 ± 0.010	6.570 ± 0.050
SL-2	6.177 ± 0.002	6.507 ± 0.005	6.183 ± 0.005	6.505 ± 0.003
SL-3	6.180 ± 0.020	6.480 ± 0.020	6.150 ± 0.030	6.470 ± 0.030

[a] Undistorted ZB MnTe: $a = 6.346 \pm 0.002$ Å (present study).

pared with two calculated data sets, corresponding to (i) spins perpendicular to the AF sheets, and (ii) an "in-plane" spin orientation with an equal distribution between two orthogonal directions—which may be either the Keffer structure, or a coexistence of two collinear substates within the "X" domain family. The reliability index R is defined as follows:

$$R = \frac{\sum |I_{\text{obs}} - I_{\text{cal}}|}{\sum I_{\text{obs}}}. \tag{3}$$

As can be seen from Table IV, the observed intensities definitely rule out the former model, and agree quite well with the latter ones. Taking into account that powder diffraction studies on β-MnS[11] and experiments on MnSe/ZnSe[38] superlattices also indicate an "in-plane" spin orientation in these systems, our present results lead to the conclusion that such an AFM-III arrangement is common for all ZB Mn chalcogenides.

An important objective of our experiments was the characterization of the AF phase transition in ZB MnTe. The temperature dependence of the square of the staggered magnetization $M(T)$ in the MnTe spin sublattice obtained from measurements of the AFM-III reflection intensities vs T is displayed in Fig. 4. As noted, our measurements have revealed a certain temperature shift in the population of inequivalent domain states. Instead of plotting the usual $M(T) = \sqrt{P(T)/P(T \to 0)}$ data obtained from studying a single magnetic reflection (where P denotes the integrated intensity), we have assumed that in such a case $M(T)$ is proportional to the sum of magnetic diffraction intensities from each domain type. In view of our discussion in the preceding part of this section, a practical definition of $M(T)$ becomes

$$M(T) \propto \sqrt{P_{01\frac{1}{2}}(T) + 2P_{0\frac{1}{2}1}(T)}. \tag{4}$$

At lower temperatures the $M(T)$ data follow the mean-field Brillouin function corresponding to a Néel temperature $T_0 = 88$ K. However, the character of this dependence visibly changes around $T \approx 60$ K, and the intensity falls sharply to zero at $T = 67$ K. Such an abrupt disappearance of the AF order in the system is a clear signature of a *first-order* phase transition. Additional supporting evindence for that is a weak hysteresis in the magnetization observed near the transition point. As noted, a first-order phase transition has been predicted to occur in this class of AFM-III systems by the renormalization-group theory. So far, the only experimental evidence for that has been provided by powder diffraction studies of β-MnS.[11] The results of the present study on MnTe further confirm the universality of this theory. In fact, the shape of the transition characteristics seen in both these systems is strikingly similar, except that the MnTe data exhibit some "smearing," and this effect is far less visible in the β-MnS data. Such rounding is most probably caused by weak residual stresses which are still present in the films, as indicated by the x-ray data. It is well known that anisotropic strain leads to a shift in the phase-transition temperature, so that nonuniform stresses usually produce

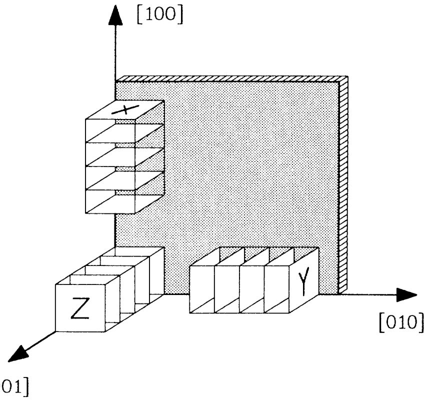

FIG. 3. A scheme illustrating the orientation of the AF sheets in three possible AFM-III domain configurations in an epitaxial layer grown on a (001) substrate. While in a bulk system these three states are equivalent, in an epitaxial layer the energy-spin for the "Z" configuration may be different from the "X"and "Y" configurations due to anisotropy in spin-spin coupling resulting from strain effects.

TABLE IV. Comparison of the $(0k\frac{n}{2})$ magnetic reflection integrated intensities observed in a MnTe film, with calculated intensities corresponding to two different spin orientations.

Reflection indices *hkl*	Relative intensity: Measured data	 Calculated for spins: In xy plane	 Along z
$01\frac{1}{2}$	26.1	26.1	26.1
$01\frac{3}{2}$	25.7	28.2	7.7
$01\frac{5}{2}$	19.5	18.8	2.1
$01\frac{7}{2}$	11.5	9.8	0.6
$03\frac{1}{2}$	8.0	8.1	11.6
$03\frac{3}{2}$	8.8	7.6	7.6
Reliability index R:		6.3%	51.3%

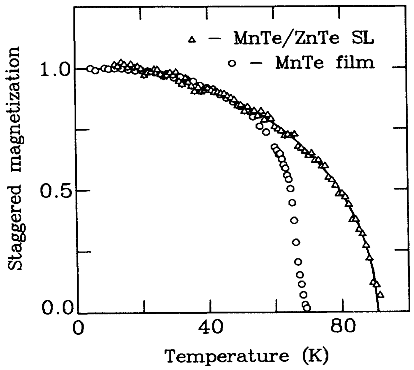

FIG. 4. Staggered magnetization vs T in a "semibulk" MnTe film (circles), and in strained MnTe layers in a MnTe/ZnTe superlattice (triangles). The data were obtained by studying the temperature dependence of the AFM-III reflections (see text). The solid curve is the mean-field Brillouin function for $S = \frac{5}{2}$ fitted to the superlattice data.

a similar rounding. However, although the magnitude of the strain effects in the MnTe films can be estimated from the broadening of the x-ray reflections, a quantitative evaluation of the smearing effects still poses a problem, because there is practically no information about the strain dependence of the phase-transition temperature. A reasonable assumption may be that the *order of magnitude* of this coefficient in MnTe is the same as in MnO ($\sim$ 2 K/kbar), one of the few fcc antiferromagnets in which the strain shift of the first-order phase-transition temperature has been thoroughly studied.[48] Taking into consideration the lattice distortion in MnTe as indicated by the x-ray peak broadening, and the existing estimates of elastic constants in ZB MnTe,[50] one can conclude that the stress in the epilayers is 0.5–1 kbar, which indeed may produce a smearing of similar magnitude as observed in Fig. 4.

B. MnTe/ZnTe superlattices: The effect of strain

The crystalline quality of the MnTe/ZnTe superlattices has been thorougfully investigated for samples SL-1 and SL-2. Diffraction scans in Q space carried out along directions parallel to the [001] growth axis (a "map" of all diffraction scans discussed in this section is displayed in Fig. 5) revealed characteristic groups of superlattice peaks occurring at regular intervals ΔQ in the vicinity of Bragg reflections points for bulk unstrained ZnTe and MnTe. Examples of such data obtained from measurement on sample 1 near the (002) and (022) reflections are shown in Fig. 6, and near the (020) reflection in Fig. 7. For both samples the superlattice period $D = \Delta Q/2\pi$ obtained from diffraction measurements was in good agreement with that expected from the RHEED oscillations.

The intensity of the nuclear reflections was analyzed by fitting $|F_{\rm BL}|^2$ "envelopes" (see Appendix B) to the peak patterns. Since the lattice periods $c_{\rm MnTe}$ and $c_{\rm ZnTe}$ in the growth direction cannot be determined by direct measurements, these quantities are treated in the fits as adjustable parameters. The results of fits are shown in Fig. 6 as thick solid curves. It should be noted that in the case of the (002) spectrum this procedure yields quite accurate $c_{\rm MnTe}$ values. This is due to the fact that the coherent scattering amplitudes $b_{\rm coh}$ of Te and Zn happen to be very similar (5.43 fm and 5.68 fm, respectively[51]), whereas there is a big difference between the scattering amplitudes of Te and Mn [the latter is -3.73 fm (negative)]. Hence, in the vicinity of $\mathbf{Q} = (0, 0, 4\pi/c_{\rm ZnTe})$ the interference term in the bilayer structure factor [Eq. (B3)] describing the scattering from ZnTe layer is strongly suppressed, whereas the MnTe layer term is enhanced. Consequently, the shape and maximum position of $|F_{\rm BL}(Q_z)|^2$ is not particularly sensitive to the value of $c_{\rm ZnTe}$, so that the fit yields unambiguous $c_{\rm MnTe}$ data. The "in-plane" lattice parameter a_{xy} can be obtained in a straightforward way by carrying out a $(0, \xi, 0)$ diffraction scan (i.e., corresponding to symmetric transmission geometry). The profile of the (020) reflection from the superlattice structure seen in sample SL-2 is shown in Fig. 8. This peak is only slightly broader than the (020) reflection from the nearly perfect GaAs substrate recorded in the same measurement, showing that there is a well-established "common" lattice periodicity in the multilayer plane (see Appendix B and Fig. 16).

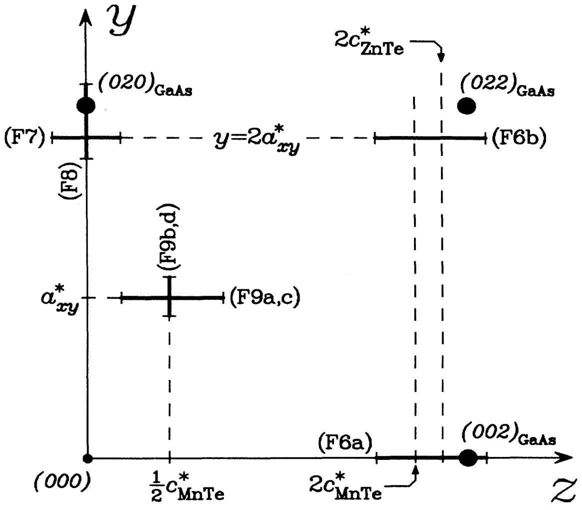

FIG. 5. A "map" of the YZ plane in Q space, illustrating the scanning trajectories (the thick "bars") for the data shown in Figs. 6–9. The symbols in parentheses (F6a, etc.) indicate the number of the corresponding figure. The large black circles are the reflection points of the GaAs substrate, and a^*_{xy}, $c^*_{\rm MnTe}$, and $c^*_{\rm ZnTe}$ are the reciprocal lattice periods for the strained MnTe and ZnTe layers in the superlattice structure (see text).

As in our previous studies of MnSe/ZnSe multilayers, a search for magnetic reflections in MnTe/ZnTe superlattices carried out at low temperatures revealed only one family of AFM-III peaks—namely, the $(0k\frac{2n+1}{2})$ series. Diffraction scans performed at other symmetry-related AFM-III points showed no detectable evidence of magnetic scattering. Another analogy with the MnSe/ZnSe

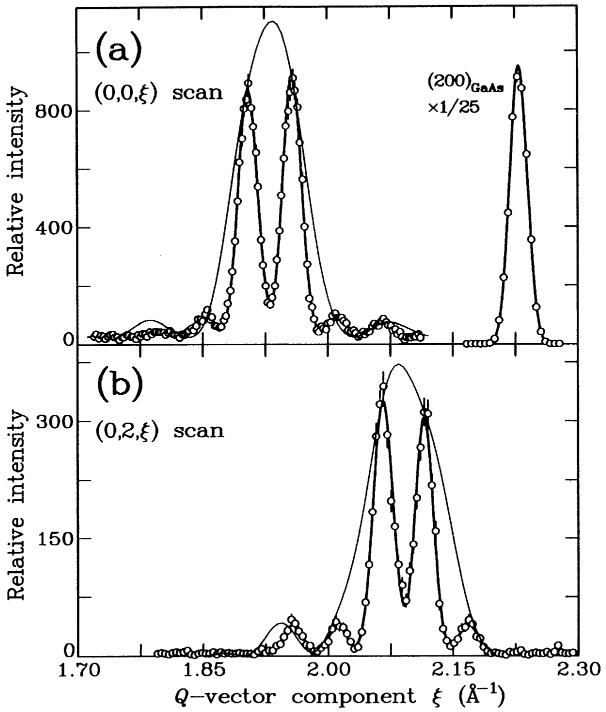

FIG. 6. Diffraction data from a MnTe/ZnTe multilayer (sample SL-2) obtained by performing scans parallel to the [001] direction in Q space. The data show characteristic groups of evenly spaced superlattice peaks occurring near the positions of the (002) and (022) Bragg reflections for bulk unstrained materials. The thin solid curves are the calculated single bilayer structure factor squares corresponding to a given scan (see Appendix B). The plots show that the observed sequences of the superlattice peak intensities are well described by these "envelope" functions.

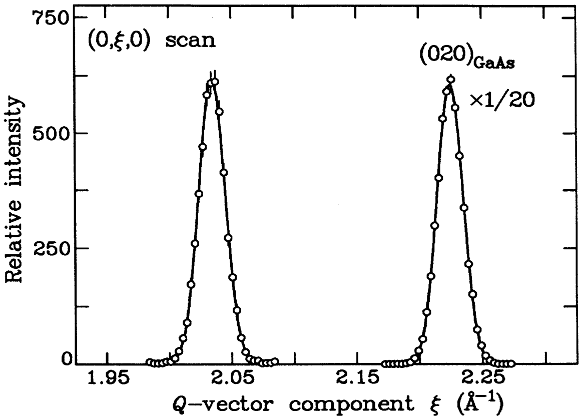

FIG. 8. Diffraction scan through the center of the middle peak in Fig. 7 parallel to the [010] direction (left side of the plot). From the position of this peak one can determine the value of the "common" lattice parameter for MnTe and ZnTe in the growth plane. By extending the scan toward higher ξ values, one can also observe the (020) reflection from the GaAs substrate (right side of the plot). The widths of these two peaks show essentially no differences, indicating a very good crystalline quality of the superlattice structure in the growth plane.

data is the width of the magnetic peaks observed in scans along various directions in Q space (Fig. 9). Scans along the [010] direction [Figs. 9(b) and 9(d)] show essentially no intrinsic broadening, indicating long-range order in the plane of the layers, with a range $>$ 1000 Å. In contrast, the peak profiles obtained by scanning parallel to the [001] direction [Fig. 9(a) and 9(c)] are always visibly broadened, and here their width in Q space clearly correlates with the MnTe layer thickeness (L), showing good agreement with the known Debye relation, $\Delta Q \approx 0.94\frac{2\pi}{L}$. In other words, the data show that—as might be expected—the range of the AFM-III spin ordering in the growth direction simply corresponds to the magnetic layer thickness. This behavior is consistent with the very short range of the AF interaction in MS systems which rules out any "communication" between the magnetic layers through the relatively thick diamagnetic ZnTe spacers. Another indication of the lack of interlayer coupling is the absence of any interference features in the magnetic diffraction: if there were any coherence between the spin directions in separate layers, this would manifest itself in the form of similar multipeak patterns as those seen in nuclear diffraction.

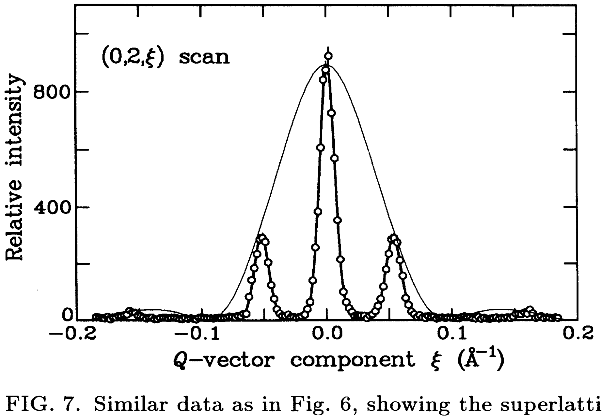

FIG. 7. Similar data as in Fig. 6, showing the superlattice peaks occurring near the (020) Bragg position.

The occurrence of *only one* family of AFM-III reflections indicates the stabilization of a unique domain orientation in the MnTe layers—namely, the one with the AF sheets *parallel* to the plane of the layers (all three topologically possible domain configurations are illustrated in Fig. 10). Such a preference is clearly a direct consequence of strain. As indicated by the a_{xy} and c_{MnTe} lattice parameter data given in Table III, the MnTe lattice exhibits a considerable tetragonal distortion, with the $(c-a)/a$ ratio of around 6%. This distortion results in different NN exchange interactions parallel and perpendicular to the epilayer plane ($J_{\|}$ and $J_{\perp}$, respectively). The interaction energy per spin in the configuration with the AF sheets parallel to the layer plane is then $-8J_{1\|}$, while that for the two configurations with the AF sheets perpendicular to the layer plane is $-8J_{1\perp}$. It is expected that the strength of the exchange coupling increases with shortening of the bond length—i.e., that $J_{1\parallel} > J_{1\perp}$. Hence, the former configuration leads to a lower magnetic energy than the latter ones, thus explainng the observed preference.

As follows logically from the above model, a tetragonal distortion with $(c-a)/a < 1$ in the magnetic layers should change this preference and stabilize domains with the AF sheets *perpendicular* to the layer plane [i.e., as shown in Fig. 10(b)]. It is therefore worth mentioning that this type of distortion occurs in another recently grown superlattice system, MnSe/ZnTe, and neutron-diffraction data from these multilayers indeed show such an orientation of the sheets. In fact, the strain-induced anisotropy in J produces in this case even more dramatic changes, such as helical arrangements of the sheets. This effect can also be explained in the framework of the same simple model, thus providing additional support for our approach. However, for details the reader is referred to the original papers on the subject.[31,32]

The most striking difference between strained and unstrained MnTe layers arises in the order of the phase transition. This is illustrated in Fig. 4 which, in addition to the magnetic reflection intensity vs T for a MnTe epilayer, also shows analogous data obtained for one of the MnTe/ZnTe superlattices. As seen in this figure, at lower temperatures the data from both systems follow a very similar mean-field Brillouin-squared function. However, in contrast to the abrupt deviation from this dependence that occurs in the case of the epilayer data, the data from the superlattice closely follow the Brillouin-squared curve over the entire T range below the Néel point. Identical behavior, which is typical for the systems undergoing a second-order AF phase transition, is observed in MnSe/ZnSe multilayers. In this latter case we have attributed the second-order nature of the transition to strain effects, but this interpretation could not be verified by comparing with data from unstrained ZB MnSe.

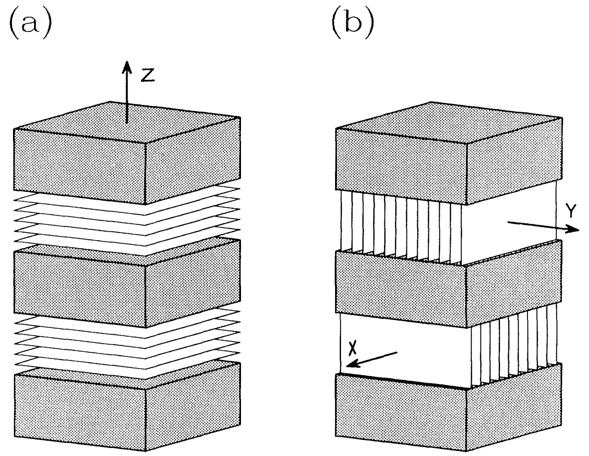

FIG. 10. Topologically possible AFM-III domain states in a (001) multilayer system. The shaded blocks symbolize the nonmagnetic layers. (a) the AF sheets are parallel to the magnetic layer plane, which is equivalent to the "Z" domain configuration defined in Fig. 2. (b) the sheets are perpendicular to the layer plane—here there are two equivalent "X"and "Y" configurations. Our experiments show that in the MnTe/ZnTe multilayers the AF sheets are always parallel to the MnTe layer planes.

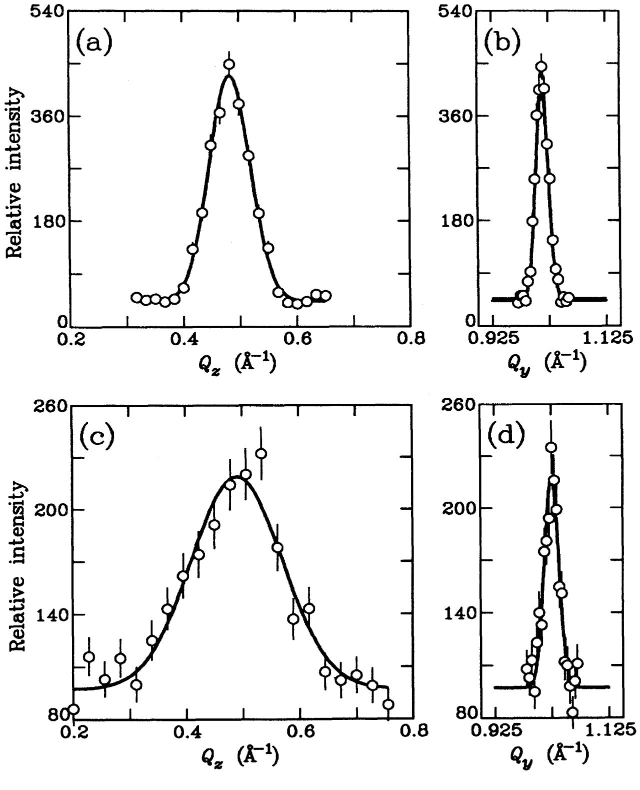

FIG. 9. Diffraction scans through the centers of the $(0, 1, \frac{1}{2})$ magnetic reflections in superlattice sample SL-1 and SL-2 in two perpendicular directions. The profiles obtained from scanning along the Y direction [plots (b) and (d)] show only a slight broadening beyond the instrumental resolution width, indicating a long range of the AFM-III spin correlations within the layer plane. In contrast, the profiles observed in scans along the Z direction [plots (a) and (c)] are strongly broadened, and their widths in Q space clearly correspond to thicknesses of the MnTe layers in the superlattices.

The present data from epitaxial MnTe systems, which show a first-order transition in the unstrained films, and a second-order in strained layers, provide direct evidence that the change of the phase transition is indeed the result of strain. It should be stressed that the change of the phase-transition order cannot be explained as the result of lowered system dimensionality because the magnetic peak intensity vs T characteristics from all three superlattice specimens clearly show the same behavior (see Fig. 11), even though the magnetic layer thicknesses in samples 3 and 1 differ by a factor of 13. Also, the change of the transition order cannot be interpreted as a secondary effect resulting from a change of the spin structure. Such an alternative explanation requires additional attention, because the renormalization-group theory predicts a first-order transition only if the spins are *parallel* to the plane of the AF sheets, but permits a second-order transition if the spins are *perpendicular* to these sheets.

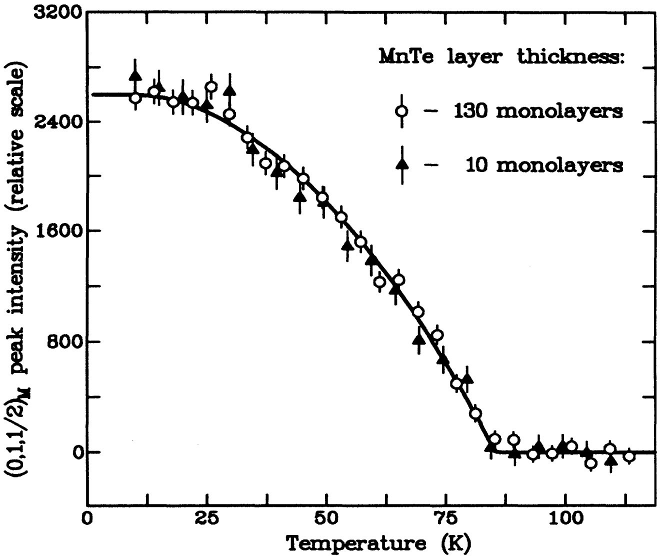

FIG. 11. A comparison of the magnetic peak intensities vs T for two MnTe/ZnTe superlattices with MnTe layer thicknesses corresponding to 10 and 130 monolayers (samples SL-1 and SL-3, respecively). As shown by the figure, both data sets can be fitted by the same squared Brillouin function (solid curve), indicating that there is no significant dependence of the Néel temperature on the layer thickness for $L \geq 10$ monolayers.

It is tempting to speculate that the strain might produce a uniaxial magnetic anisotropy and flip the spin orientation. However, the analysis of magnetic peak intensities rules out such a mechanism, showing that in the superlattices the spins also remain confined to planes of the AF sheets.

C. $Zn_{1-x}Mn_xTe$ epitaxial films: The effect of dilution

X-ray diffraction tests performed on the $Zn_{1-x}Mn_xTe$ films show that the crystalline quality of these ternary epitaxial systems is only slightly worse than the quality of pure MnTe films. The rocking curves are somewhat broader ($\sim 0.3°$) than those obtained from the MnTe specimens, but such a mosaic spread, or even larger, is typically seen in bulk single crystals of $A^{\mathrm{II}}_{1-x}\mathrm{Mn}_xB^{\mathrm{VI}}$ alloys. Some additional peak broadening was also observed in the $\theta - 2\theta$ scans. This broadening may indicate somewhat larger residual stresses than in the case of pure MnTe, as well as small fluctuations in the material composition which change the lattice parameter slightly. From the observed peak widths $\Delta\theta$ we find that the inhomogeneity in x is not larger than $\sim$1.5%.

Scans over the magnetic reflection points at low T revealed the formation of all three possible AFM-III domain types in the investigated samples. In all cases the observed $(0k\frac{1}{2})$ reflections were roughly twice as intense as the $(0\frac{1}{2}l)$ reflections, indicating the same preferred domain orientation as in the case of undiluted films.

In the two samples with the lowest Mn concentrations (x=0.695 and 0.725) the peak width is visibly broadened with respect to the crystalline peaks, indicating a limited range of the magnetic order. The correlation length $\xi = \kappa^{-1}$ deduced from the peak width is $\sim$ 100 Å. This is consistent with the behavior observed in bulk samples of $Zn_{1-x}Mn_xTe$ and $Cd_{1-x}Mn_xTe$ with similar concentrations,[21,25] and establishes the equivalence of both growth techniques. For all samples investigated with higher Mn concentrations ($x \geq 0.815$) the magnetic peaks are essentially of the same width as the crystalline peaks, showing that in this x region the AFM-III LRO is well established.

The results of studies of temperature dependence of the magnetic scattering intensity $P_M(T)$ in the $Zn_{1-x}Mn_xTe$ films are listed in Table I. Examples of the measured data from some of the samples (with x = 0.725, 0.85, 0.938, and for pure MnTe) are shown in Fig. 12. The shape of the $P_M(T)$ characteristics for the films with x=0.85 (Fig. 12) and 0.815 shows a good agreement with the mean-field Brillouin-squared function for all temperatures below the Néel point, thus indicating a *second-order* transition to a LRO AFM-III phase. There is a marked difference, however, in the case of the samples with x = 0.938 (Fig. 12) and higher, which all exhibit a much sharper falloff of the magnetization as one approaches the Néel temperature. We attribute this to the fact that in this range of x the magnetic phase transition crosses over to *first order.* The results of $Zn_{1-x}Mn_xTe$ film studies are summarized in Fig. 13, where the Néel temperatures obtained from the magnetic intensity vs T data are plotted as a function of Mn concentration. The

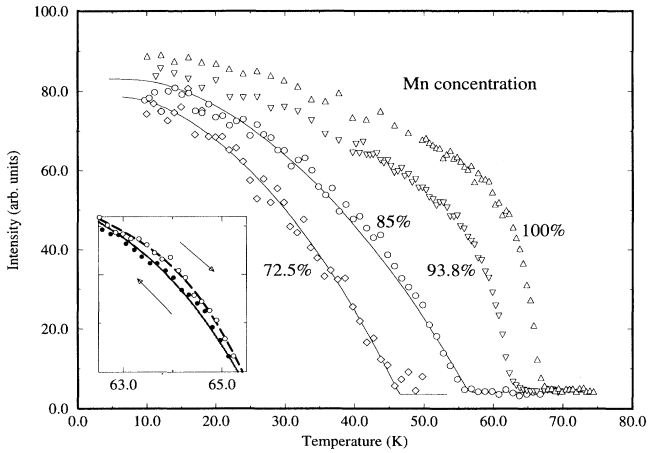

FIG. 12. Examples of the temperature dependence of the $(01\frac{1}{2})$ magnetic peak intensity for $Zn_{1-x}Mn_xTe$ films with several different x values. For the samples with x = 0.725 and 0.85 the transition is of second order, and agrees well with the Brillouin square mean-field formulas for Mn^{2+} spin $S = \frac{5}{2}$ (solid lines), and Néel temperature 46.5 and 56.4 K, respectively. The 93.8% and 100% concentration samples exhibit different behavior, indicating a first-order phase transition. The inset shows a slow (1 K/h) scan with increasing (open circles) and decreasing (dark circles) T near the transition temperature in the pure MnTe sample, showing a small magnetization hysteresis.

shaded vertical stripes in this (x, T_c) phase diagram indicate the expected locations of the boundaries between the SRO and LRO antiferromagnetic phases, and between the two LRO phases. The existence of both these phase boundaries has been theoretically predicted,[17] and our data provide the first qualitative experimental confirmation of such a double-crossover scheme. Figure 13 also shows for comparison the magnetic susceptibility cusp temperatures obtained from experiments[19] on bulk alloy samples with $x \leq 0.68$.

D. Magnetostriction in MnTe films

The availability of MnTe single-crystal films has made possible high-resolution x-ray measurements of the lattice parameter in the magnetically ordered phase. Mo and Cu $K\alpha$ radiation was used, and we investigated (0,0,4), (0,0,6), (0,0,8), and (0,0,12) peaks in the symmetric reflection geometry. Very tight slit settings (0.05 mm and 0.1 mm before and after the sample, respectively) were used in order to obtain the best possible resolution.

Typical scans reveal three peaks: from MnTe, ZnTe buffer, and GaAs. Each of these peaks is doubled, due to the $K\alpha_I$ and $K\alpha_{II}$ components of the Cu $K\alpha$ line. The most interesting results occur in the low-T region, below the AFM-III transition temperature: we observe the splitting of the MnTe peak (Fig. 14). This splitting decreases with increasing temperature. Its magnetic origin was confirmed by warming the sample above T_N and subsequent cooling—the splitting disappeared above T_N, and then reappeared below T_N with the same magnitude. The relative magnitude of the lattice spacing difference corresponding to the low-T splitting is approximately 0.3%.

We attribute this splitting to magnetostriction within the AFM-III domains. As noted, the neutron data indicate that at $T = 10$ K about 55–60 % of the sample volume forms domains of the "Z" type, and the remaining volume is devided between domains of the "X" and "Y" types (see Fig. 3). The x-ray diffraction measures the lattice constant in the [001] direction, and the splitting indicates that there are regions in the sample with slightly different (001) interplanar spacing. There is a clear correlation between the relative intensities of the two split x-ray peak components, and the relative population of the "Z" and the two symmetry-equivalent "X" and "Y" domain states. Such behavior suggests that the peak splitting is caused by a magnetostriction mechanism

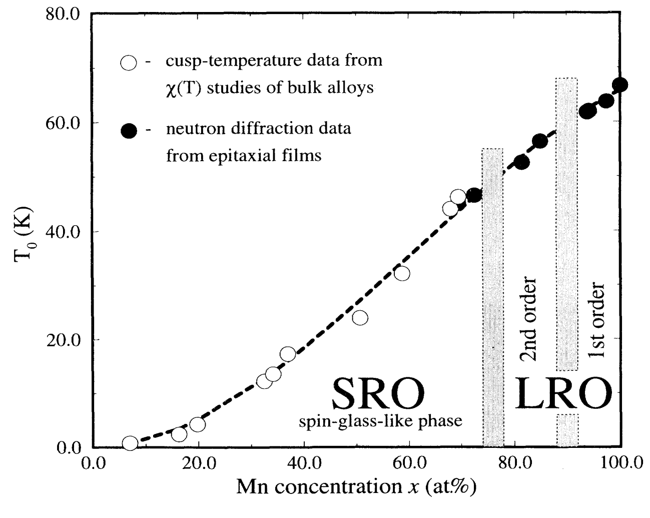

FIG. 13. AF phase-transition temperature of MBE $Zn_{1-x}Mn_xTe$ films obtained from neutron-diffraction measurements (full data points), plotted together with the traditional magnetic phase diagram obtained by mapping the the cusp temperature data (empty circles) from magnetic susceptibility experiments on bulk $Zn_{1-x}Mn_xTe$ crystals for the range $x \leq 0.68$ (after Ref. 19). The dashed curve is a guide for the eye, and the shaded contours indicate the expected positions of the boundaries between short-range ordered (SRO) and long-range ordered (LRO) AF phases, and between LRO phases undergoing first-order and second-order phase transitions.

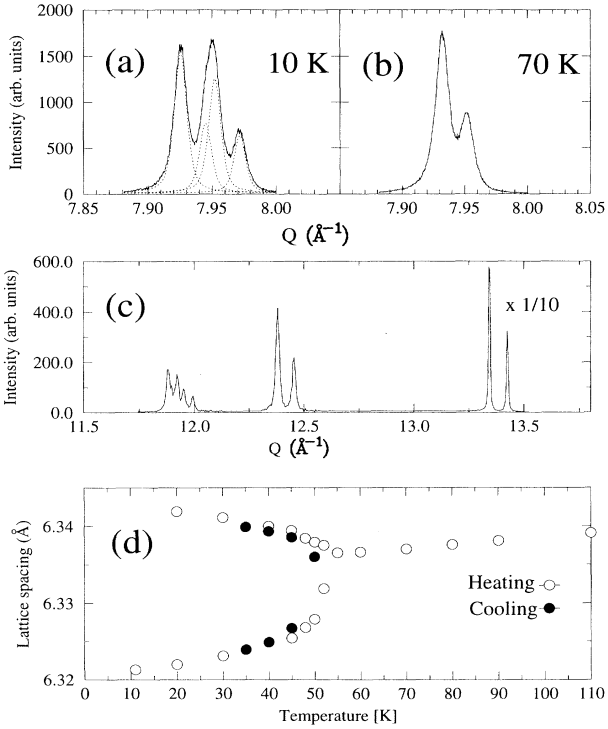

FIG. 14. (a) and (b) high-resolution x-ray diffraction data from a single-crystal MnTe film, showing magnetostriction splitting of the (8,0,0) reflection at low T (the two peaks in the 70 K data are resolved Cu $K\alpha_I$ and $K\alpha_{II}$ lines; at low T the reflection splits into two such doublets—shown as the dotted curves—which together produce a three-peak maximum). As shown in plot (c), which displays the (12,0,0) reflections measured at 10 K using Mo $K\alpha$ radiation, there is no splitting of the reflection from the GaAs substrate ($Q \sim 13.7$ Å^{1}) and from the nonmagnetic ZnTe "buffer" layer ($Q \sim 12.8$Å^{1}). (d) The growth-direction lattice constant of MnTe calculated from both peaks of the split doublet is plotted as a function of temperature.

which tends to shorten the lengths of the AF bonds in the AFM-III structure. In fact, as indicated by many experimental observations, as well as by theoretical analyses of the exchange phenomena in $A^{\mathrm{II}}_{1-x}\mathrm{Mn}_xB^{\mathrm{VI}}$ and $\mathrm{Mn}B^{\mathrm{VI}}$ compounds, the magnitude of the Mn-Mn exchange interactions in these systems always *increases* with decreasing ion-ion distance. Hence, the shortening of the AF bonds in the ordered phase lowers the total magnetic energy, and this effect produces the contracting force.

It is important to notice, however, that this process involves only the bonds lying in the planes of the AF sheets in the AFM-III structure. Because the energies of all "out-of-plane" bonds sum up to zero, shortening of these bonds would not change the total magnetic energy. Hence, there is no contracting force in the direction perpendicular to the AF sheets. In other words, the magnetostriction decreases the (001) interplanar spacing only in the "X" and "Y" domains. This is indeed consistent with the fact that the less intense peak componenent shifts toward higher 2θ angles. This behavior is illustrated by the lower branch of the split lattice parameter characteristic in Fig. 14(c). On the other hand, as can be seen in the same figure, the peak arising from the "Z" domains exhibits a somewhat smaller shift in the *opposite* direction. This effect can also be explained on the grounds of the same model—obviously, the increase of the (001) interplanar spacing in the "Z" domains is an elastic response of the crystal lattice to the contraction which occurs in the (001) plane.

It is fair to mention, however, that some of our observations are not yet sufficiently understood. For instance, one intriguing effect is the change of the relative intensities of the split x-ray peak components. When the temperature increases, the peak corresponding to the "Z" domains increases in intensity while the other component weakens. This effects clearly indicates a temperature shift in the domain populations, and such a shift is also manifested by the aforementioned change of the intensity ratio of the $(01\frac{1}{2})$ and $(0\frac{1}{2}1)$ neutron magnetic peaks (Fig. 15). Another puzzling observation is that the sharply defined transition temperature at which the magnetostriction appears ($T = 52$ K) is different from the Néel temperature in MnTe ($T_N = 66$ K). Several experimental artefacts have been eliminated in the latter case, e.g., sample heating by x-rays. A possible explanation of both these peculiar effects is that they reflect the existence of weak residual stresses in the MnTe film, as well as the influence of the substrate on the magnetoelastic process. A small *compressive* strain in the (001) plane (which is expected because $a_{\mathrm{MnTe}} > a_{\mathrm{ZnTe}} > a_{\mathrm{GaAs}}$) would indeed favor the formation of the "Z" domains, and therefore such domains may constitute an overwhelming majority in the first stage of cooling below T_N. Notice, however, that if the film consists only of "Z-type" domains, the freedom of contraction in the AF sheet plane is strongly limited because the film is "anchored" to the massive substrate. Hence, the lowering of the total magnetic energy takes place only if other domain types begin to form. This may explain the "delay" in temperature as well as the population shift. However, such a scenario requires additional confirmation by detailed model studies, as well as experiments on MnTe films with growth directions other than [001].

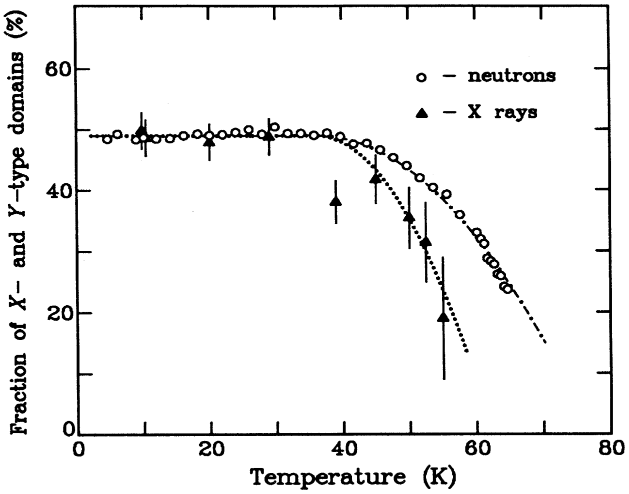

FIG. 15. The temperature shift between the populations of different AFM-III domain states in a MnTe film. The plot shows the fraction of the sample volume corresponding to the "X" and "Y" domains (see Fig. 3), as deduced from the comparison of the $(01\frac{1}{2})$ and $(0\frac{1}{2}1)$ neutron-diffraction peak intensities (open circles), and from the intensities of the split x-ray diffraction peak components (dark triangles). The curves are guides for the eye.

V. SUMMARY AND CONCLUSIONS

In summary, the application of MBE to the growth of new $A^{\mathrm{II}}_{1-x}\mathrm{Mn}_xB^{\mathrm{VI}}$ and $\mathrm{Mn}B^{\mathrm{VI}}$ systems has provided access to the previously unknown ZB forms of MnTe and MnSe. The results of the present work, as well as our previous studies of MnSe/ZnSe and MnSe/ZnTe superlattices, and of $\mathrm{Cd}_{1-x}\mathrm{Mn}_x\mathrm{Se}$, epilayers have demonstrated that neutron diffraction provides a unique tool for characterizing the details of the magnetic properties of these artificial structures.

Our data show that the spin structures occurring in all the members of the ZB Mn chalcogenide family are remarkably similar, which is consistent with our present theoretical understanding of the exchange interaction mechanisms in these compounds. One problem that still cannot be resolved by our data is whether the AFM-III structure seen in MnTe and MnSe is collinear or of Keffer type. The question concerning the existence of a significant Dzyaloshinskii-Moriya term in the spin-spin interaction therefore awaits answers from future experiments. It should be pointed out, however, that these epitaxial structures — which are *single-crystal* specimens make such studies at least conceivable. Especially the MnTe/ZnTe and MnSe/ZnTe superlattices are highly interesting systems in the context of such experiments, because here the strain already selects a single AFM-III domain state—a major advantage in studying noncollinear phenomena. It still remains a problem of how to force all the spins to choose only one of the two collinear substates in the case the structure is truly collinear, or how to unequivocally prove that it is canted. Here diffraction studies in strong external magnetic fields may hold the answer. It should be noted, however, that some preliminary experiments done by us on MnTe/ZnTe superlattices and MnTe films at 6 T showed no detectable changes of the magnetic peak intensities, suggesting that even stronger fields may be required to perturb the the spin system.

The comparison of the data obtained from MnTe films and MnTe/ZnTe superlattices clearly demonstrates that strain has a profound influence on static ordering effects as well as on the phase-transition mechanism in the frustrated spin system. In particular, the observation of the change of the phase-transition order in a distorted lattice provides additional support for the renormalization-group theory interpretation of the phase transition mechanism in fcc antiferromagnets based on symmetry arguments. It has been already shown, e.g., by experiments on MnO, that lowering of the lattice symmetry leads to a shift in the order of the phase transition.[48] However, no direct proof has been obtained before for an AFM-III system. So far, we were able to demonstrate that using a system in which the deviation from cubic symmetry was particularly strong ($c/a \approx 1.06$), the discontinuity in the phase transition is totally removed. It would be certainly of even greater interest to investigate the intermediate stages of the process—i.e., a gradual "weakening" of the first-order transition as a function of lattice distortion. Current progress in the MBE growth raises hopes that such experiments can be done in the near future, using superlattices with a controlled strain magnitude in the MnTe layers, e.g., through the growth of systems with ternary nonmagnetic layers, such as MnTe/$\mathrm{Zn}_{1-x}\mathrm{Cd}_x$Te. Since $a_{\mathrm{ZnTe}} = 6.10$ Å, $a_{\mathrm{CdTe}} = 6.49$ Å, and in $\mathrm{Zn}_{1-x}\mathrm{Cd}_x$Te the lattice parameter is a linear function of x, by changing the x value one can tailor the lattice mismatch between the superlattice constituents, and thus "tune" the strain in the MnTe layers to desired values.

Our studies of the films have made it possible for the first time to determine a magnetic phase diagram of an $A^{\mathrm{II}}_{1-x}\mathrm{Mn}_xB^{\mathrm{VI}}$ system *in the entire* $0 < x \leq 1$ range. The exact composition where the LRO↔SRO transition occurs, as well as the position of the boundary between the areas characterized by a first-order and by a second-order transition is now a matter of studying additional samples within the $0.70 < x < 1$ concentration region. Furthermore, the information already at hand concerning the phase-transition temperatures for $x > 0.70$ contains some remarkable implications. The data plotted in Fig. 13 certainly suggest that the T_0 vs x characteristic for $\mathrm{Zn}_{1-x}\mathrm{Mn}_x$Te is rather featureless—in particular, it does not appear likely that there is any pronounced anomaly in this curve corresponding to the LRO-SRO phase boundary. This behavior, if confirmed by further data, would mean that in the SRO phase the system retains a surprisingly strong "memory" of the T_0 characteristic of the LRO phase—which may be an argument against the spin-glass nature of the SRO phase, and in favor of the activated dynamics model and the dynamically inhibited AF transition concepts oulined in Ref. 28.

Let us finally comment on the importance of our observation of magnetostriction in the MnTe films. Although exchange striction in antiferromagnets is a well-known phenomenon and is known to have a direct or indirect influence on many of their properies, this effect has been usually neglected or ignored in analyses of $A^{\mathrm{II}}_{1-x}\mathrm{Mn}_xB^{\mathrm{VI}}$ and $\mathrm{Mn}B^{\mathrm{VI}}$ magnetism. The results of our x-ray measurements show that there is little justification for this. Especially the shift in domain population—if confirmed by further studies—may have very far reaching consequences for our understanding of antiferromagnetism in $A^{\mathrm{II}}_{1-x}\mathrm{Mn}_xB^{\mathrm{VI}}$ systems in its LRO as well as SRO forms. In particular, this would mean that magnetostriction determines the domain structure of the LRO phase. Furthermore, since our present picture of the breakdown of the LRO around $x \approx 0.70$ is based on the formation of a large number of domainlike "clusters,"[19] it may appear that magnetostriction also plays an important role in this case, in addition to topological disorder that has been so far believed to be totally responsible for this effect. One more practical aspect of magnetostriction studies is that they potentially offer a way for directly determining the dJ/dr values. So far, no measured dJ/dr data are available for $A^{\mathrm{II}}_{1-x}\mathrm{Mn}_xB^{\mathrm{VI}}$ and $\mathrm{Mn}B^{\mathrm{VI}}$ compounds, and such information would be extremely helpful for quantative interpretations of other magnetoelastic phenomena seen in these system, such as, e.g., the newly discovered strain-induced helimagnetism in MnSe/ZnTe multilayers.[31,32]

ACKNOWLEDGMENTS

This work was supported by NSF Grant Nos. DMR 8821635 and DMR 9121353.

APPENDIX A: DIFFRACTION IN COLLINEAR AND CANTED AFM-III SYSTEMS

As can be clearly seen in Figs. 2(b) and 2(c), the magnetic unit cell in the AFM-III structure is the fcc cell doubled along the direction perpendicular to the AF sheets. By calculating the magnetic structure factor[51]

$$F^{\mathrm{mag}}_{hkl} = \sum_{\mathrm{mag.\ cell}} S_j e^{2\pi i(hu_j + kv_j + lw_j)} \tag{A1}$$

for the simplest collinear configuration (where $S_j = \pm 1$ for "up" and "down" spins, and u_j, v_j, w_j are the ion coordinates in the magnetic unit cell) one can readily find that the selection rules for the AFM-III reflections (expressed in normal cubic coordinations) are the following: the index corresponding to the cell doubling direction is a half-integer ($l = \frac{2n+1}{2}$), and of the remaining two h, k indices one is an even integer, and one an odd integer (e.g., $10\frac{1}{2}$, $01\frac{5}{2}$, $21\frac{3}{2}$, etc.).

The integrated intensity of a reflection from a single-crystal sample with a collinear AF structure can be written as

$$P(hkl)_{\rm mag} \propto \frac{f^2(Q)}{\mathcal{L}} |F_{hkl}^{\rm mag}|^2 \sin^2 \alpha, \tag{A2}$$

where $f(Q)$ is the form factor of the magnetic ion, α is the angle between the reciprocal lattice vector $\boldsymbol{\tau}_{hkl}$ and the direction of the magnetic moments, and $\mathcal{L}$ is the Lorentz factor depending on the scan type. In collinear AFM-III order the value of $|F_{hkl}^{\rm mag}|$ is the same for all (hkl) reflections. Hence, if the spins are perpendicular to the AF sheets (i.e., parallel to the cell doubling direction), the reflection intensity is

$$P(hkl)_{\rm mag} \propto \frac{f^2(Q)}{\mathcal{L}} \frac{h^2+k^2}{h^2+k^2+l^2}, \tag{A3}$$

and if the spins are parallel to the AF sheets and oriented in the direction of a unit vector $\widehat{\boldsymbol{\sigma}} = (\xi, \eta, 0)$, then

$$P(hkl)_{\rm mag} \propto \frac{f^2(Q)}{\mathcal{L}} \left(1 - \frac{(h\xi + k\eta)^2}{h^2+k^2+l^2}\right). \tag{A4}$$

However, it is a realistic expectation that in the latter case the crystal will contain equal populations of collinear domain states with two orthogonal spin orientations, $\widehat{\boldsymbol{\sigma}}' = (\xi, \eta, 0)$ and $\widehat{\boldsymbol{\sigma}}'' = (-\eta, \xi, 0)$. By averaging Eq. (A4) we obtain the following expression for the observed reflection intensity:

$$P(hkl)_{\rm mag} \propto \frac{f^2(Q)}{2\mathcal{L}} \left(1 + \frac{l^2}{h^2+k^2+l^2}\right). \tag{A5}$$

As follows from the above, the AFM-III structures with spins parallel and perpendicular to the AF sheets can be easily distinguished through measurements of reflection intensities. However, the problem becomes more complicated if we consider noncollinear arrangements, such as the Keffer structure. In such cases, the simple scalar term $|F_{hkl}^{\rm mag}|^2 \sin^2 \alpha$ in Eq. (A2) should be replaced by a more complicated vector expression $|\mathbf{F}_{hkl}^{\rm mag}|^2$, where

$$\mathbf{F}_{hkl}^{\rm mag} = \sum_{\rm mag\ cell} [\mathbf{K}_j - \boldsymbol{\epsilon}(\boldsymbol{\epsilon} \cdot \mathbf{K}_j)] e^{2\pi i(hu_j + kv_j + lw_j)}, \tag{A6}$$

where $\boldsymbol{\epsilon}$ is a unit vector parallel to $\boldsymbol{\tau}_{hkl}$, and $\mathbf{K}_j$ is a unit vector in the direction of the spin of the jth ion. It is quite straightforward to check that in the case of the Keffer arrangement Eq. (A6) leads to an identical expression for reflection intensity as Eq. (A5). Hence, the Keffer structure can be distinguished from a collinear configuration only if the measurements are done on a truly *single-domain* specimen, and the creation of such experimental conditions may pose a challenging problem even in the case of a single-crystal sample.

APPENDIX B: NUCLEAR DIFFRACTION IN SUPERLATTICES MADE UP OF ZB MATERIALS

Let us consider a superlattice consiting of alternating layers of two ZB materials, with a (001) growth axis. In a simple kinematical approach[52] (which is fully justified in the case of presently discussed systems because of their relatively small thicknesses and significant lattice distortion effects), the intensity observed in a diffraction scan along the [001] direction in Q space is given by the following equation:[53]

$$I(Q_z) \propto \frac{\sin^2 \frac{NDQ_z}{2}}{\sin^2 \frac{DQ_z}{2}} |F_{\rm BL}(Q_z)|^2, \tag{B1}$$

where N is the total number of bilayers, D is the bilayer thickness, and Q_z is the z component of the scattering vector $\mathbf{Q} = (0, 0, Q_z)$. $F_{\rm BL}(Q_z)$ is the structure factor of a "bilayer unit cell," defined as

$$F_{\rm BL}(Q_z) = \sum_{j=1}^{n} \varrho_j e^{iz_j Q_z}, \tag{B2}$$

where the sum is over all n (001)-type atomic planes comprising the bilayer, ϱ_j is the "scattering density" of the jth plane (i.e., the total scattering amplitude for unit area), and z_j is its coordinate along the [001] axis.

The first right-hand factor in Eq. (B1), which is a well-known function from the general theory of diffraction phenomena, describes the *positions* of the Bragg reflections from the superlattice structure. This function peaks at Q_z values which are integral multiples of $2\pi/D$. The $|F_{\rm BL}(Q_z)|^2$ factor is an "envelope" function describing the reflection *intensities.* It forms broad maxima ($\delta Q_z > 2\pi/D$) in the vicinity of Bragg reflection points for the bulk systems, and is essentially zero everywhere else. Hence, in Q scans parallel to the [001] direction one observes characteristic groups of several evenly spaced ($\delta Q_z = 2\pi/D$) superlattice peaks.

The arrangement of cation and anion planes in a single bilayer is shown schematically in Fig. 16. A ZB crystal with cubic lattice parameter a can be looked upon as being built up of "molecular monolayers," each consisting of a single (001) cation plane and a single anion plane, $a/4$ apart. The separation between two consecutive monolayers of this kind in the [001] direction is $a/2$. Let us denote the [001] lattice periods of the two superlattice constituents as c_1 and c_2 (due to the strain effects, these parameters may be somewhat different from the normal cubic lattice constants). The bilayer structure factor for

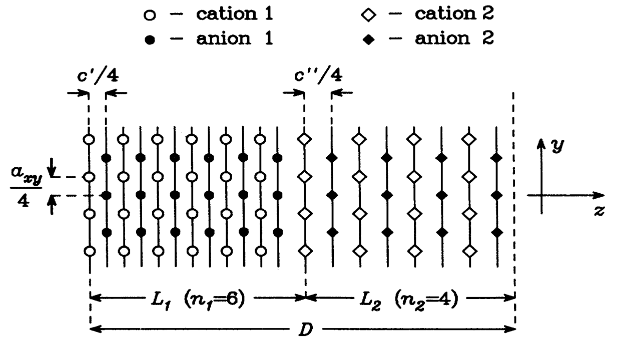

FIG. 16. The arrangement of cation and anion planes in a single bilayer composed from two different ZB materials, as seen when looking along the [100] direction.

a (001) ZB superlattice can then be written as

$$F_{\rm BL} \propto \sum_{j=0}^{n_1-1} \{ b_1^C e^{iQ_z j \frac{1}{2} c_1} + b_1^A e^{iQ_z (j+\frac{1}{2}) \frac{1}{2} c_1} \} + \sum_{k=0}^{n_2-1} \{ b_2^C e^{iQ_z [L_1 + l \frac{1}{2} c_2]} + b_2^A e^{iQ_z [L_1 + (l+\frac{1}{2}) \frac{1}{2} c_2]} \}, \tag{B3}$$

where n_1,n_2 is the number of molecular monolayers in each of the two constituents layers, $b_1^C, \ldots$, etc., are the scattering amplitudes of the cation and anion nuclei in each of the layers, and $L_1 = n_1 c_1$ is the thickness of the first layer (i.e., the z coordinate of the first cation plane in the second layer).

In systems such as Mn-VI/II-VI multilayers the mismatch between the magnetic and nonmagnetic lattices is relatively large (4–5 %). This leads to a significant distortion from cubic symmetry in both materials. Due to the epitaxy condition at the (001) layer interface, the "in-plane" lattice spacing (a_{xy}) in one of the materials is reduced, and is increased in the other material to match one another. As a result, the lattice spacings in the [001] direction must, respectively, increase or decrease to accomodate the elastic strain (Fig. 17). While the value of (a_{xy}) is easily measured by transmission geometry diffraction, an accurate determination of c_1 and c_2 may not be trivial. This is because the $|F_{\rm BL}(Q_z)|^2$ function has sometimes a highly asymmetric shape, and fitting it as an "envelope" to the measured peak intensities leads to ambiguous c_1 and c_2 values due to a strong correlation between the parameters. However, the fit reliability may radically improve if one of the terms in Eq. (B3) is strongly dominant — as happens, e.g., in the MnTe/ZnTe multilayers near the (002) reflection point.

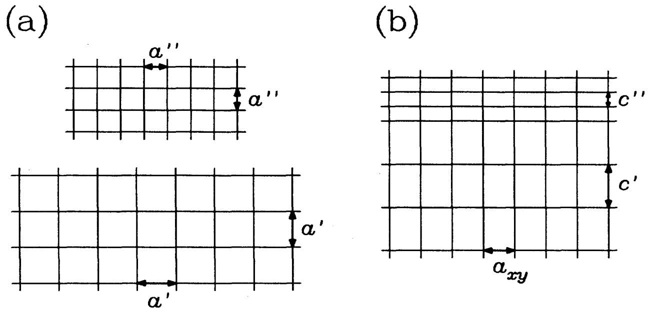

FIG. 17. Plot explaining the lattice distortion effects taking place in the MnTe/ZnTe superlattices: (a) constituent lattices with different periodicities $a' > a''$; (c) a bilayer in which the in-plane parameters match up to form a common periodicity. Then $a' < a_{xy} < a''$, while the lattice parameters in the z direction get elongated ($c' > a'$) and contracted ($c'' < a''$), respectively.

---

[*] Present address: University of Maryland, College Park, MD 20742.

[†] Present address: Pennsylvania State University, University Park, PA 16802.

[1] B. E. Larson, K. C. Haas, H. Ehrenreich, and A. E. Carlsson, Phys. Rev. B **37**, 4137 (1988).

[2] A. Lewicki, J. Spalek, J. K. Furdyna, and R. R. Galazka, Phys. Rev. B **37**, 1860 (1988).

[3] A. Bruno and P. Lascaray, Phys. Rev. B **38**, 9168 (1988).

[4] B. E. Larson, K. C. Haas, and R. L. Aggarwal, Phys. Rev. B **33**, 1789 (1986).

[5] A. Oleś, F. Kajzar, M. Kucab, and W. Sikora, *Magnetic Structures Determined by Neutron Diffraction* (Państwowe Wydawnictwo Naukowe, Kraków, 1976).

[6] J. Lynn, G. Shirane, and M. Blume, Phys. Rev. Lett. **37**, 154 (19).

[7] J. Hastings, N. Elliott, and L. M. Corliss, Phys. Rev. **115**, 13 (1959).

[8] T. Chattopadhyay, T. Bruckel, and P. Burlet, Phys. Rev. B **44**, 7394 (1991).

[9] A. Annila, K. Clausen, A. Oja, J. Touriniemi, and H. Weinfurter, Phys. Rev. B **45**, 7772 (1992).

[10] L. Corliss, N. Elliott, and J. Hastings, Phys. Rev. **104**, 924 (1956).

[11] J. Hastings, L. Corliss, W. Kunnmann, and D. Mukamel, Phys. Rev. B **24**, 1388 (1981).

[12] L. A. Kolodziejski, R. L. Gunshor, N. Otsuka, B. P. Gu, Y. Hefetz, and A. V. Nurmikko, Appl. Phys. Lett. **48**, 1482 (1986).

[13] S. M. Durbin *et al.*, Appl. Phys. Lett. **55**, 2087 (1989).

[14] K. Binder and A. P. Young, Rev. Mod. Phys. **58**, 801 (1986).

[15] F. Keffer, Phys. Rev. **126**, 896 (1962).

[16] C. L. Henley, Phys. Rev. Lett. **62**, 2056 (1989).

[17] G. S. Grest and E. F. Gabl, Phys. Rev. Lett. **43**, 1182 (1979).

[18] J. A. Fernandez, H. A. Farah, C. P. Poole, and M. Puma, Phys. Rev. B **27**, 4274 (1983).

[19] J. K. Furdyna and N. Samarth, J. Appl. Phys. **61**, 3526 (1987).

[20] J. K. Furdyna, J. Appl. Phys. **64**, R29 (1988).

[21] *Semiconductors and Semimetals*, edited by J. K. Furdyna and J. Kossut (Academic, New York, 1988), Vol. 25.

[22] N. Bloembergen and T. J. Rowland, Phys. Rev. **97**, 1679 (1955).

[23] L. de Seze, J. Phys. C **10**, L 353 (1977).

[24] J. Villain, Z. Phys. B **33**, 31 (1979).

[25] T. M. Giebultowicz and T. M. Holden (Ref. 21), Chap. 4, pp. 125–181.

[26] R. R. Galazka, S. Nagata, and P. H. Keesom, Phys. Rev. B **22**, 3344 (1980).

[27] S. Oseroff and P. H. Keesom, (Ref. 21), Chap. 3, pp. 73–123.

[28] S. Geschwind, A. T. Ogielski, G. E. Devlin, J. Hegarty, and P. Bridenbaugh, J. Appl. Phys **63**, 3738 (1988).

[29] T. M. Giebultowicz, P. Kłosowski, N. Samarth, H. Luo, J. J. Rhyne, and J. K. Furdyna, Phys. Rev. B **42**, 2582 (1990).

[30] T. M. Giebultowicz, J. J. Rhyne, W. Y. Ching, D. L. Huber, J. K. Furdyna, B. Lebech, and R. R. Galazka, Phys. Rev. B **39**, 6857 (1989).

[31] T. M. Giebultowicz, P. Kłosowski, J. J. Rhyne, N. Samarth, H. Luo, and J. K. Furdyna, Physica B **180-181**, 485 (1992).

[32] T. M. Giebultowicz, N. Samarth, H. Luo, P. Kłosowski, J. K. Furdyna, and J. J. Rhyne, Phys. Rev. B **46**, 12 076 (1992).

[33] K. Ando, K. Takahashi, and T. Okuda, J. Magn. Magn. Mater. **104-107**, 992 (1992).

[34] K. Ando, K. Takahashi, T. Okuda, and M. Umehara, Phys. Rev. B **46**, 12289 (1992).

[35] P. Kłosowski, T. M. Giebultowicz, J. J. Rhyne, N. Samarth, H. Luo, and J. K. Furdyna, J. Appl. Phys. **70**, 6221 (1991).

[36] P. Kłosowski, T. M. Giebultowicz, N. Samarth, H. Luo, J. K. Furdyna, and J. J. Rhyne, Physica B **180-181**, 114 (1992).

[37] P. Kłosowski, T. M. Giebultowicz, N. Samarth, H. Luo, J. K. Furdyna, and J. J. Rhyne, J. Magn. Magn. Mater. **104-107**, 1795 (1992).

[38] N. Samarth, P. Kłosowski, H. Luo, T. M. Giebultowicz, J. K. Furdyna, B. Larson, and N. Otsuka, Phys. Rev. B **44**, 4701 (1991).

[39] S. K. Chang, D. Lee, H. Nakata, A. V. Nurmikko, L. A. Kolodziejski, and R. L. Gunshor, J. Appl. Phys. **62**, 4835 (1987).

[40] D. Mukamel and S. Krinsky, Phys. Rev. B **13**, 5065 (1976); **13**, 5078 (1976).

[41] P. Bak and D. Mukamel, Phys. Rev. B **13**, 5086 (1976).

[42] P. W. Anderson, Phys. Rev. **79**, 705 (1950); see also J. J. Smart (Ref. 54).

[43] J. S. Smart, *Studies in Physics and Chemistry* (Saunders, Philadelphia, 1966).

[44] C. L. Henley, J. Appl. Phys. **61**, 3962 (1987).

[45] P. Bak, S. Krinsky, and D. Mukamel, Phys. Rev. Lett. **36**, 52 (1976); **36**, 829 (1976).

[46] M. Kerszberg and D. Mukamel, Phys. Rev. Lett. **43**, 293 (1979).

[47] M. Kerszberg and D. Mukamel, Phys. Rev. B **23**, 3943 (1981); **23**, 3953 (1981).

[48] D. Bloch, D. Hermann-Ronzaud, C. Vettier, W. B. Yelon, and R. Alben, Phys. Rev. Lett. **35**, 963 (1975).

[49] D. R. Yoder-Short, U. Debska, and J. K. Furdyna, J. Appl. Phys. **58**, 4056 (1985).

[50] P. Maheswaranathan, R. J. Sladek, and U. Debska, Phys. Rev. B **31**, 5212 (1985).

[51] G. E. Bacon, *Neutron Diffraction*, 3rd ed. (Clarendon, Oxford, 1975).

[52] B. Warren, *X-Ray Diffraction* (Addison-Wesley, Reading, MA, 1969).

[53] R. W. Erwin, J. J. Rhyne, M. B. Salomon, J. Borchers, S. Sinha, R. Du, J. E. Cunningham, and C. P. Flynn, Phys. Rev. B **35**, 6808 (1987).

[54] J. J. Smart, Phys. Rev. **86**, 968 (1952).